Exploring the Earth

NORSAR Scientific Report No. 2-2013

Semiannual Technical Summary

1 July – 31 December 2013

Tormod Kværna (Ed.)

Kjeller, June 2014

NORSAR

6.2 Infrasound signal detection from the Drevja accidental explosion

6.2.1 Background

We have undertaken an initial modelling effort in order to predict travel times for infrasound phases recorded at the new IS37 array. We are still in the knowledge build-up stage and more work needs to be done for us to establish a more robust arrival-time prediction framework.

In the following preliminary results, a ray-tracing engine was applied to the atmospheric conditions along the great circle path from the Drevja accidental explosion on December 17, 2013 to the new IS37 array. For comparison, we also made similar simulations for the two other Norwegian infrasound arrays ARCI and NRSI.

This analyzed ground-truth event was due to an exploding lorry carrying 15 tons of slurry. It took place at 65.988°N, 13.343°E at around 14h26 (UTC). The great circle distances from the event to the operating Fennoscandian infrasound arrays are listed in Table 6.2.1, while the sizes and geographic locations of these arrays are illustrated in Figure 6.2.1. Signals recorded at the Fennoscandian infrasound arrays as well as the Apatity infrasound array in northwest Russia are shown in Figure 6.2.2.

Table 6.2.1 – Great circle distances [km] from the Drevja event to all operating Fennoscandian infrasound arrays. Stations where ray-trace modelling is performed are typed in boldface.

LYC	Lycksele	294
KIR	Kiruna	368
IS37	**Bardufoss**	**399**
JAM	Jämtön	418
NRSI	**NORES**	**590**
SDK	Sodankylä	594
ARCI	**ARCES**	**639**

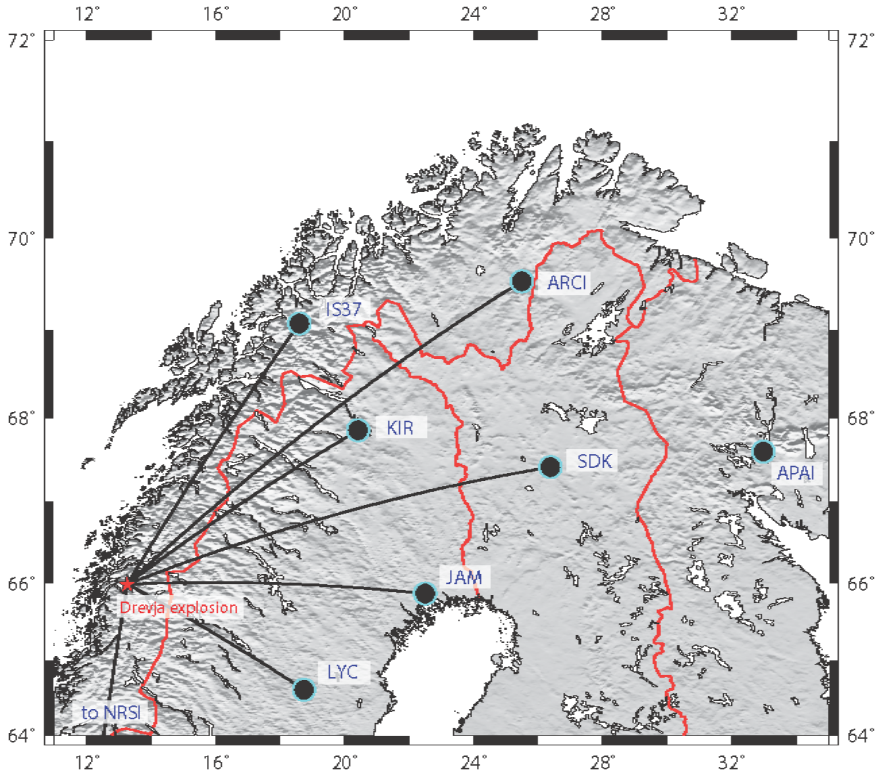

Fig. 6.2.1 The location 65.988°N, 13.343°E of the Drevja accidental explosion event in relation to the closest infrasound arrays.

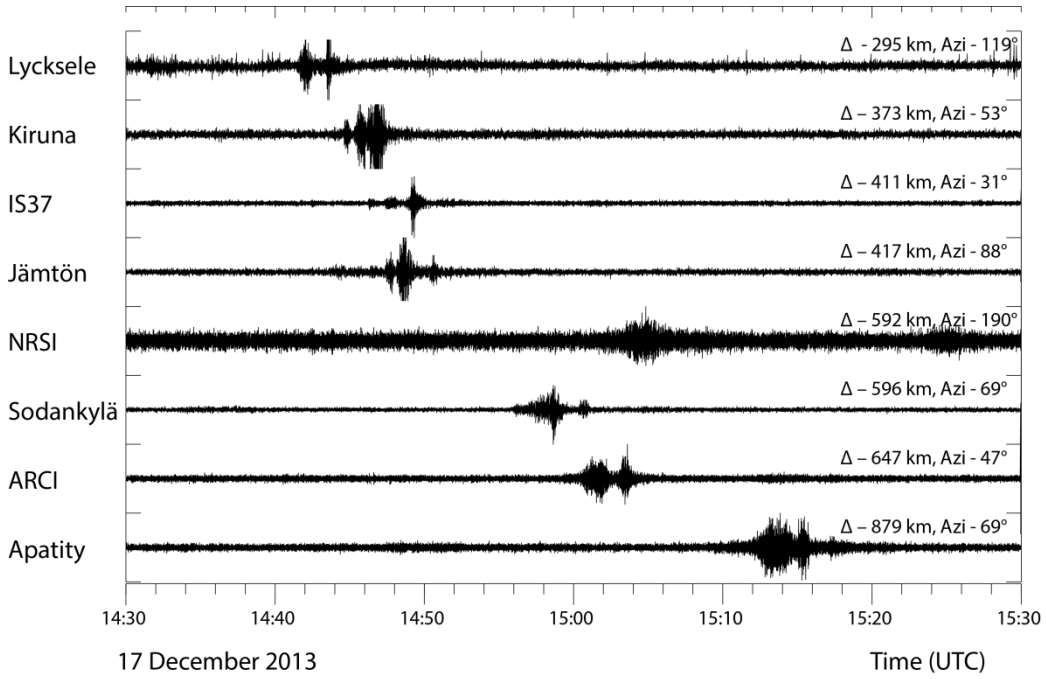

Fig. 6.2.2 Signals associated with the Drevja explosion recorded at the Fennoscandian infrasound arrays as well as the Apatity infrasound array in northwest Russia. The event-station distances and the event-station azimuth estimates are given in the right-hand side of the panel.

6.2.2 Methods

We used the Ground to Space (G2S) atmospheric model to extract wind and adiabatic sound speed profiles (Drob and Picone, 2003). This G2S model is based on the public National Oceanic and Atmospheric Administration (NOAA) global analysis fields from 0 to 45 km altitude. For altitudes between 35 and 75 km, it uses the GEOS5/MERRA public profiles published by NASA. In the overlap region, between 35 and 45 km altitude, the fields are included in the G2S profile by weighted averaging. Above 75 km, the G2S profiles are compiled from the empirical NRLMSISE-00 (temperature, see Picone et al., 2002) and HWM07 (wind, see Drob et al., 2008 and Emmert et al., 2008) models. The ray-tracing was carried out using the ART2D public code written by K. Walker at University of California, San Diego (Walker, 2012).

We refer to the different predicted infrasonic phase arrivals as tropospheric, stratospheric, and thermospheric depending on the highest altitude of the turning ray.

6.2.3 Results

For the signals recorded at the IS37 array, the signal to noise ratio (SNR) below 2 Hz is very low; it is far superior in the 2–5 Hz band. Such events demonstrate the usefulness of the array geometry with its innermost ring of closely spaced elements allowing the direction and apparent velocity of higher frequency signals to be estimated.

Figure 6.2.3 shows modelling results for the IS37 array location. Here, the ray-tracing predicts three distinct infrasound phase arrivals at ground level. Adding the corresponding travel times to the time when the explosion took place (14h26 UTC) yields: first a tropospheric arrival at around 14:46:30, then a stratospheric arrival at around 14:49:15, and finally a thermospheric arrival at around 14h50.

Looking at Figure 6.2.4, where the phase arrivals estimated by ray-tracing are indicated by vertical lines, we note that the first arrival estimate agrees with a received low-amplitude signal. The corresponding apparent velocity and back-azimuth from f-k analysis suggest that this is a tropospheric or stratospheric arrival from the direction of the event.

Similarly, the second predicted arrival corresponds well with an observed high-amplitude signal. In contrast, the third predicted arrival, which is a thermospheric phase, neither corresponds with a signal visible in the traces, nor with an increase in coherence between the element signals. The received signals also reveal a phase arrival at around 14h47. This is not directly predicted by the ray-tracing model. However, it is known that “head waves” are badly represented in ray-tracing and by using finer sampling of the ray angles, we see that the maximum range of the stratospheric first-bounce ground hit is extended. The tag “Extrapolated” in Figure 6.2.3 corresponds to such anticipated stratospheric first bounce arrivals at greater ranges than the ones shown by the plotted rays.

The apparent velocities estimated from f-k analysis looking only at correlation values exceeding 0.2 suggest that the observed phases are either stratospheric or tropospheric returns. However, as framed in green in the bottom panel of figure 6.2.4, when lowering the correlation threshold the backazimuth and apparent velocity estimates indicate a possible weak thermospheric arrival at around 14:51:30. This is around 1 minute later than what is predicted by the ray-tracing.

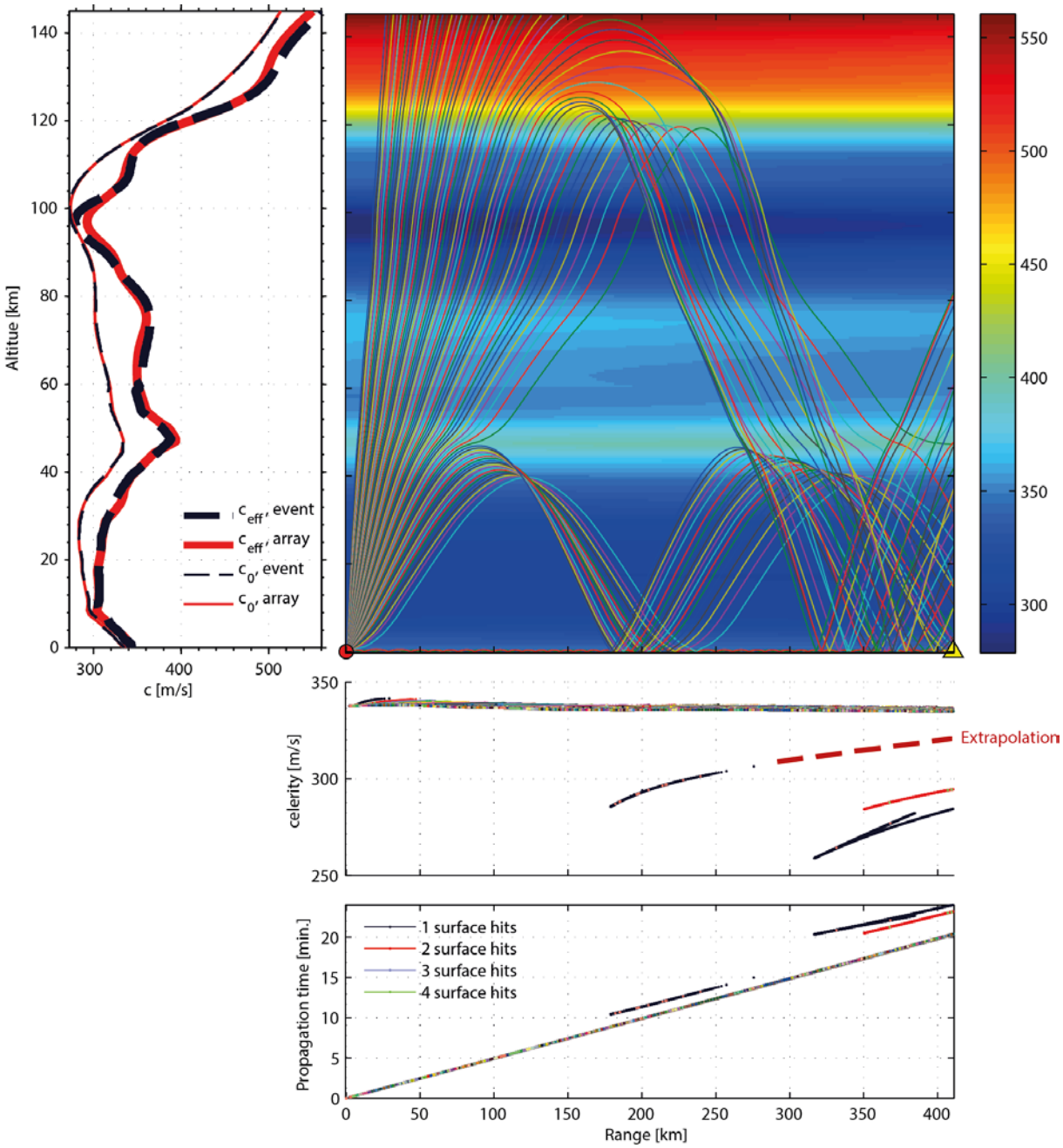

Fig. 6.2.3 Ray-trace modelling from the Drevja event to the IS37.
Top right panel: infrasound ray paths overlaid on a map of the effective sound speed $c_{eff} = c_0 + v_x$, where c_0 is the adiabatic temperature-dependent sound speed and v_x is the wind component in the direction of the great circle between the event and the array. For the predicted ground hits, the middle panel shows the corresponding celerity, while the bottom panel shows the propagation time estimate.
The tag "Extrapolated" corresponds to anticipated stratospheric first bounce arrivals at greater ranges than the ones shown by the plotted rays.
The upper left panel shows c_0 and c_{eff} profiles at the source and receiver end of the propagation path.

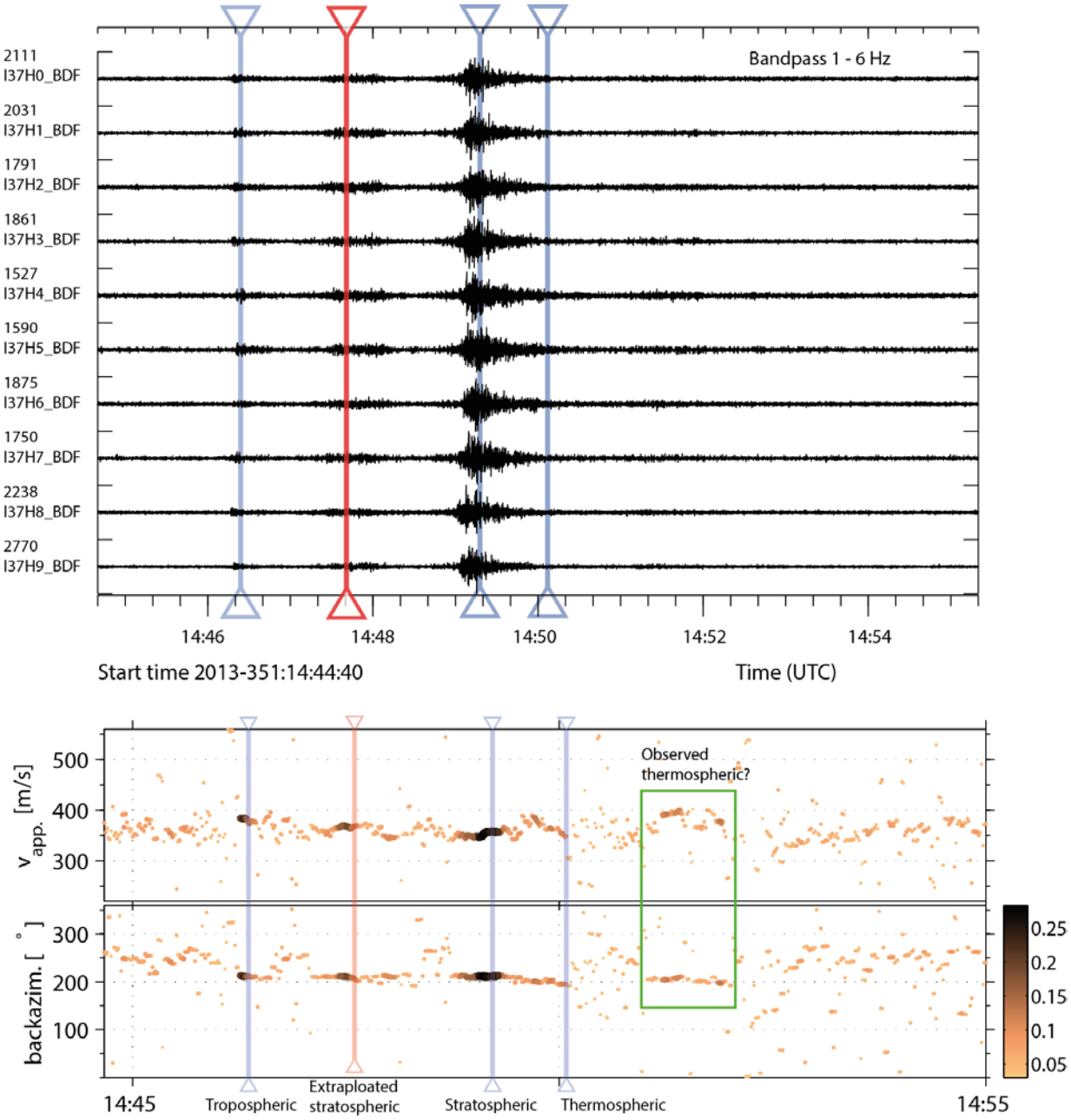

Fig. 6.2.4 The upper panel shows observations of the Drevja event at IS37, bandpass filtered between 1 and 6 Hz. Vertical lines are introduced at times when the ray-tracing predicts array arrivals (see Figure 6.2.3), where the red line represents the extrapolated stratospheric first bounce. The bottom panel shows the estimated apparent velocity and the back-azimuth from f–k analysis of the filtered received signals. The data point coloring is based on the correlation coefficient between the element signals which can be read from the colorbar. Recordings of possible thermospheric arrivals are framed in green.

For the ARCI array, the ray-tracing and signal analysis results are shown in Figures 6.2.5 and 6.2.6. Here we notice that the simulation predicts two arrivals: a tropospheric and a “double-bounce” stratospheric one. The collected data also reveals two distinct pulses. However, these are seen around 3 minutes after the predictions from ray-tracing while on the other hand the separation between them is in accordance with the simulations.

While the IS37 and ARCI arrays are located approximately north-east of the Drevja event, the NRSI array is south of it, hence making the wind along the acoustic propagation direction differ significantly. Therefore the conditions for the arrival of infrasound phases can be significantly different although the great circle distance is quite similar. Looking in Figures 6.2.7 and 6.2.8 for signals received from the event, no such are visible in the time-signal plots. But in the f-k analysis plot at around 15h05 we see a back-azimuth estimate which approximately corresponds to the direction to Drevja.

6.2.4 Conclusion

To conclude, we note that the ray-trace modelling corresponds best to the observed phase arrivals for the IS37 array. There, both a tropospheric and a stratospheric arrival are in accordance with the simulations. We need to examine whether the deviations between the model and the collected signals are mostly due to shortcomings of the ray-tracing method (which is a high-frequency approximation), or if it has more to do with the inherent inaccuracy of the atmospheric specification model.

We also plan to make similar analyses for the other infrasound arrays in the region.

Acknowledgements

We wish to thank Douglas P. Drob of the United States Naval Research Laboratory for provision of the G2S atmospheric specifications for this case study. The GEOS-5 data used in this study/project for the G2S specifications have been provided by the Global Modeling and Assimilation Office (GMAO) at NASA Goddard Space Flight Center through the online data portal in the NASA Center for Climate Simulation. The NOAA Global Forecast System (GFS) analyses fields, also for this study in the G2S specifications, are from NOAA's National Operational Model Archive and Distribution System (NOMADS), which is maintained at NOAA's National Climatic Data Center (NCDC).

References

Drob, D.P. and Picone, J.M. (2003) Global morphology of infrasound propagation. Journal of Geophysical Research, 108 (D21).

Drob, D.P., Emmert, J.T., Crowley, G., Picone, J.M., Shepherd, G.G., Skinner, W., Hays, P., Niciejewski, R.J., Larsen, M., She, C.Y., Meriwether, J.W., Hernandez, G., Jarvis, M.J., Sipler, D.P., Tepley, C.A., O'Brien, M.S., Bowman, J.R., Wu, Q., Murayama, Y., Kawamura, S., Reid, I.M. and Vincent, R.A.. (2008), An Empirical Model of the Earth's Horizontal Wind Fields: HWM07, J. Geophys Res., 113, doi:10.1029/2008JA013668.

Emmert, J.T., Drob, D.P., Shepherd, G.G., Hernandez, G., Jarvis, M.J., Meriwether, J.W., Niciejewski, R.J., Sipler, D.P. and Tepley, C.A (2008), DWM07 global empirical model of upper thermospheric storm-induced disturbance winds, J. Geophys Res., 113, doi:10.1029/2008JA013541.

Picone, J.M., Hedin, A.E., Drob, D.P. and Aikin, A.C. (2002) NRLMSISE-00 empirical model of the atmosphere: Statistical comparisons and scientific issues. Journal of Geophysical Research, 107 (A12).

Walker K. (2012) Atmospheric ray tracer 2D (ART2D). See *http://sail.ucsd.edu/~walker/software/ART2D/art2d.html*.

Sven Peter Näsholm, NORSAR

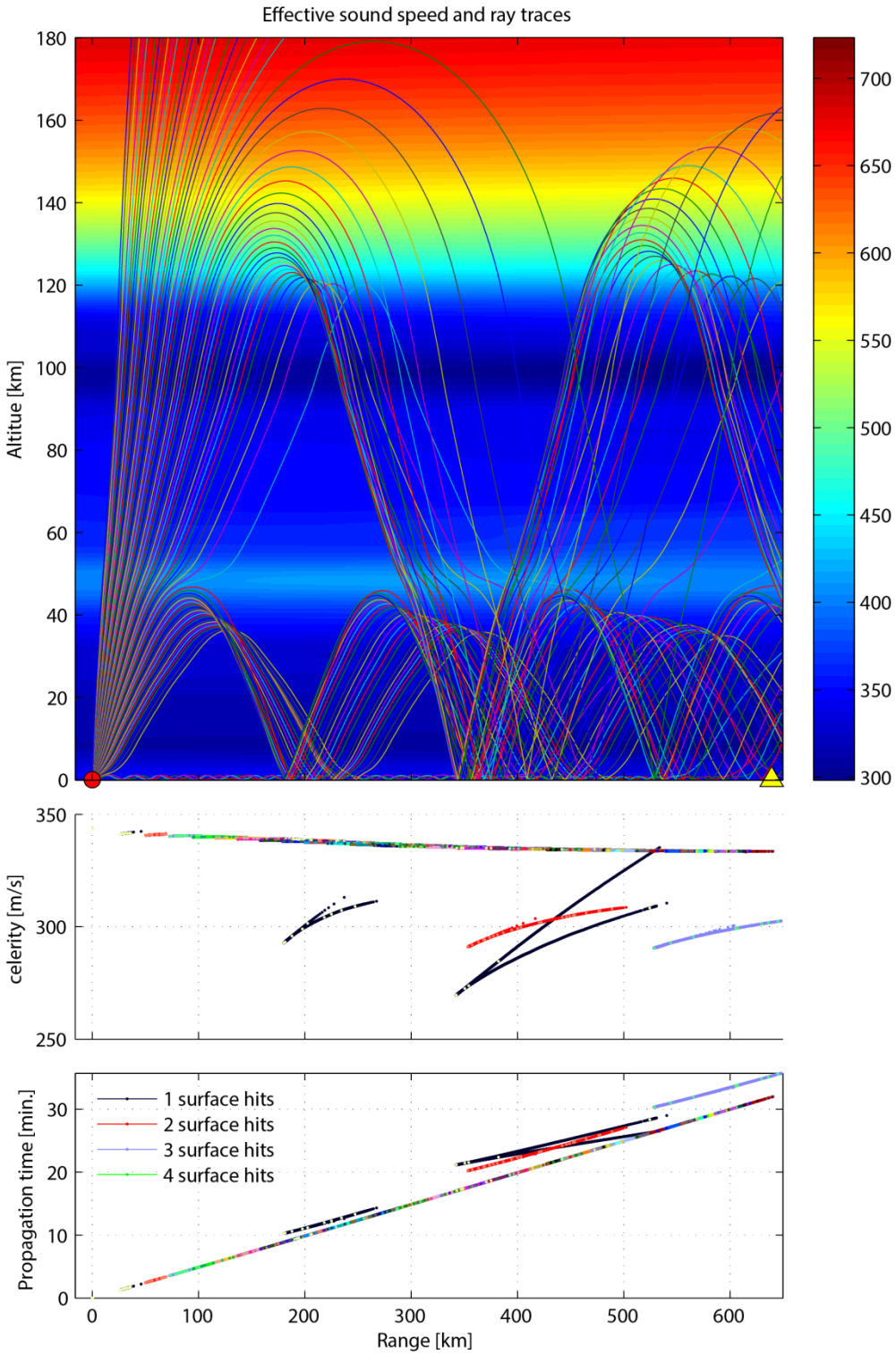

Fig. 6.2.5 Ray-trace modelling from the Drevja event to the ARCI array. Top panel: infrasound ray paths overlaid on a map of the effective sound speed $c_{eff} = c_0 + v_x$, where c_0 is the adiabatic temperature-dependent sound speed and v_x is the wind component in the direction of the great circle between the event and the array. For the predicted ground hits, the middle panel shows the corresponding celerity, while the bottom panel shows the propagation time estimate.

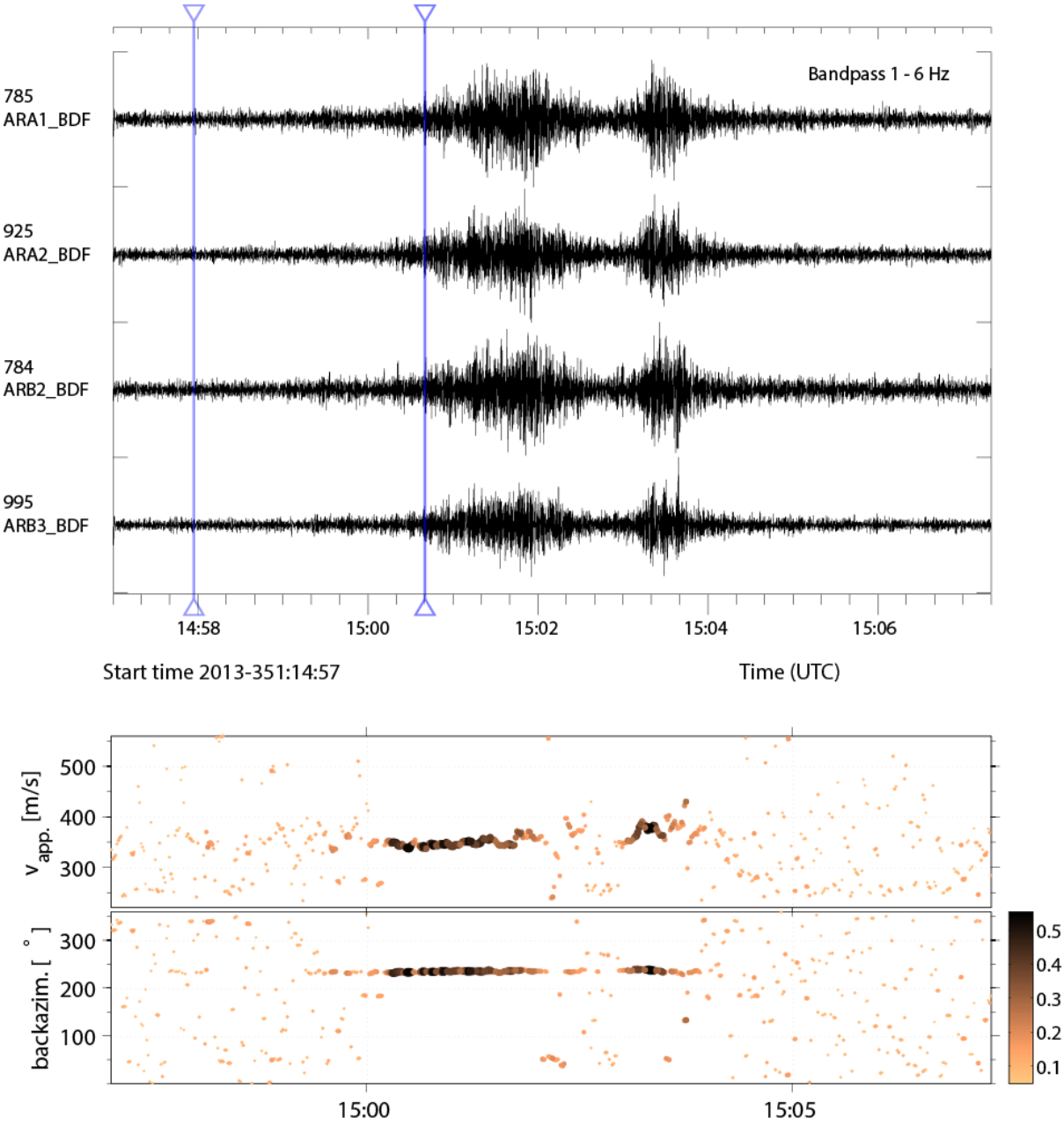

Fig. 6.2.6 The upper panel shows observations of the Drevja event at ARCI, bandpass filtered between 1 and 6 Hz. Vertical lines are introduced at times when the ray-tracing predicts array arrivals (see Figure 6.2.5).
The bottom panel shows the estimated apparent velocity and the back-azimuth from f–k analysis of the filtered received signals. The data point coloring is based on the correlation coefficient between the element signals which can be read from the colorbar.

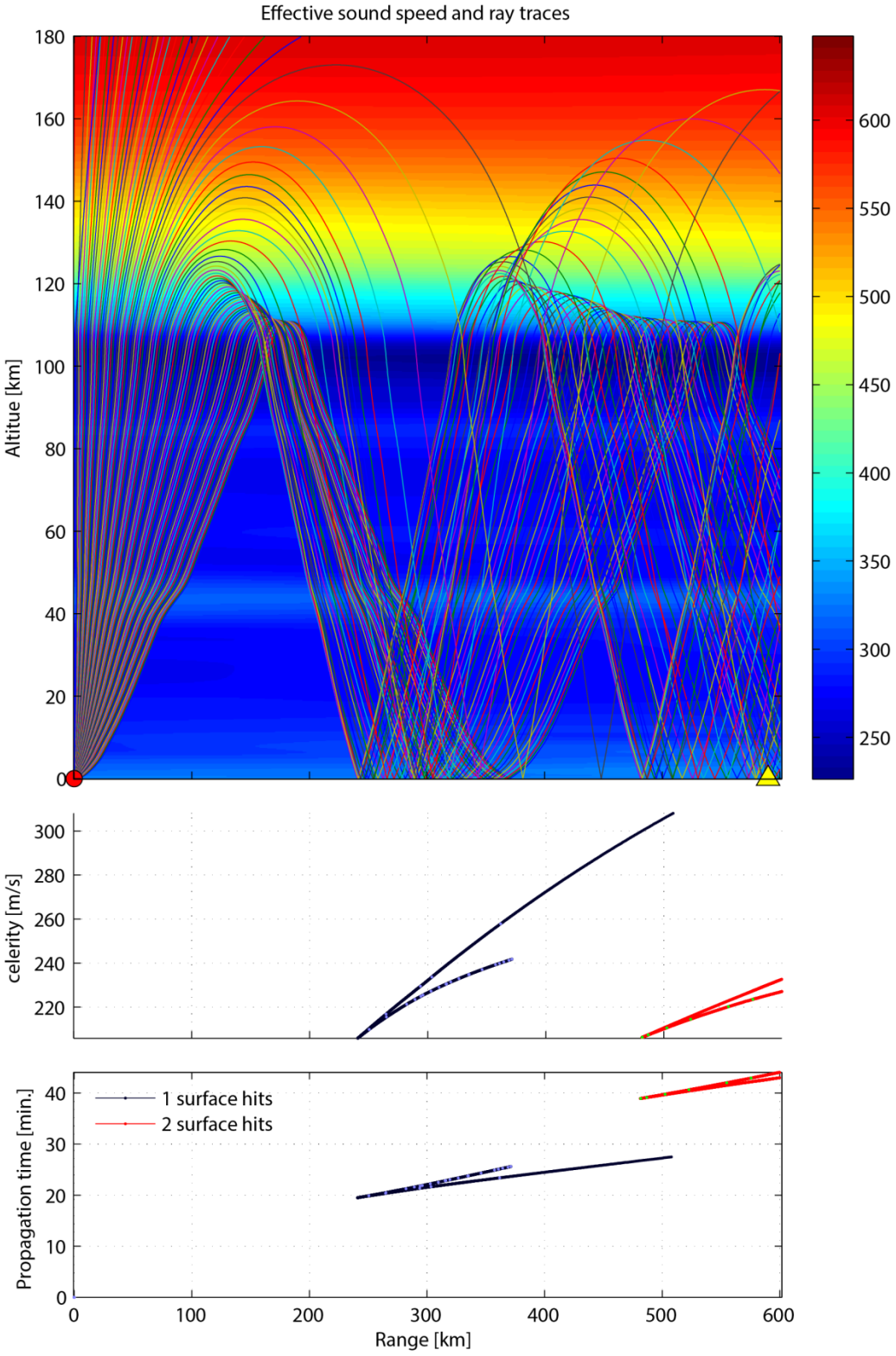

Fig. 6.2.7 Ray-trace modelling from the Drevja event to the NRSI array. Top panel: infrasound ray paths overlaid on a map of the effective sound speed $c_{eff} = c_0 + v_x$, where c_0 is the adiabatic temperature-dependent sound speed and v_x is the wind component in the direction of the great circle between the event and the array. For the predicted ground hits, the middle panel shows the corresponding celerity, while the bottom panel shows the propagation time estimate.

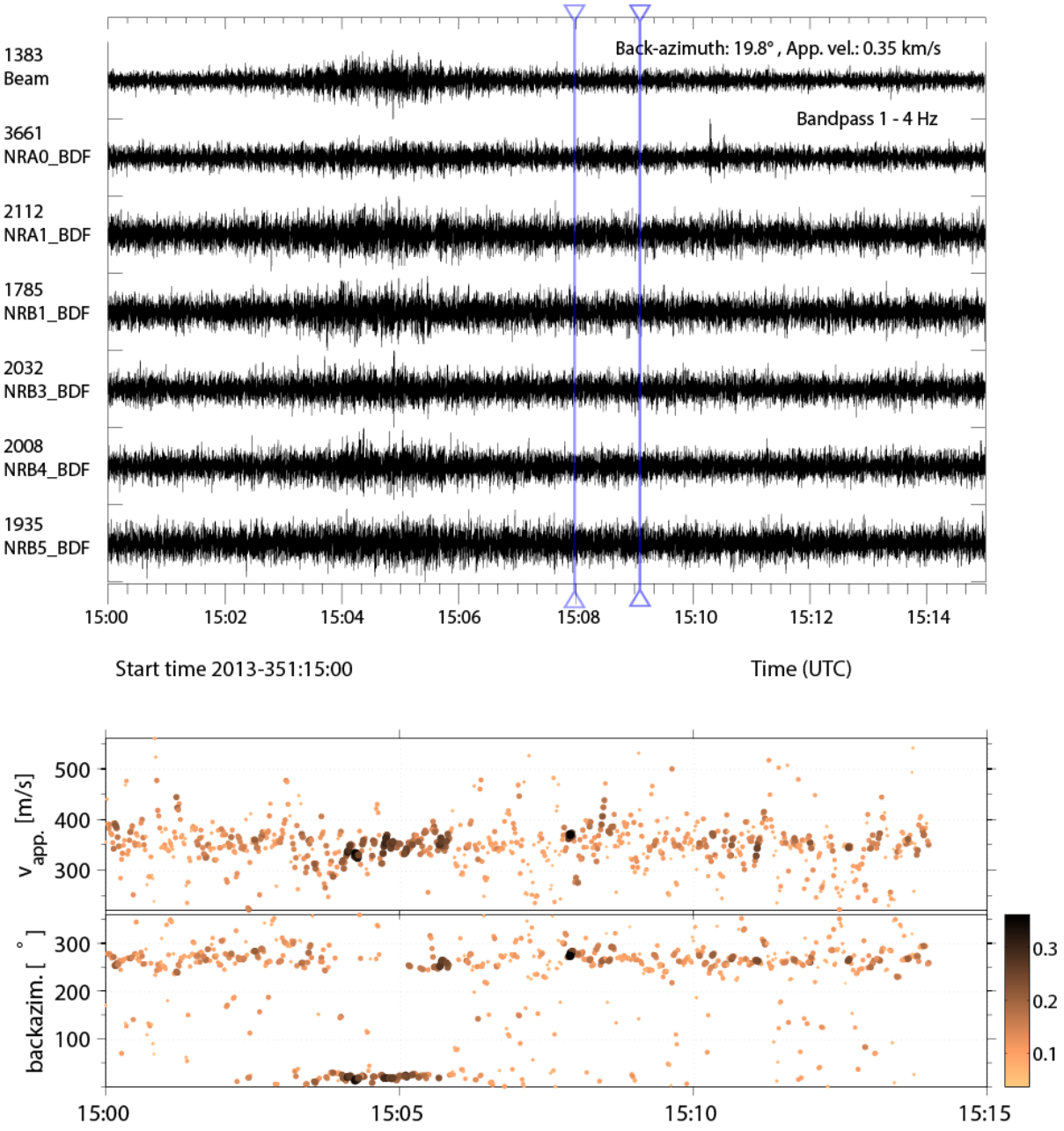

Fig. 6.2.8 The upper panel shows observations of the Drevja event at NRSI, bandpass filtered between 1 and 4 Hz. Vertical lines are introduced at times when the ray-tracing predicts array arrivals (see Figure 6.2.7).
The bottom panel shows the estimated apparent velocity and the back-azimuth from f–k analysis of the filtered received signals. The data point coloring is based on the correlation coefficient between the element signals which can be read from the colorbar. Note the increase in signal correlation and the stabilization of the back-azimuth estimate at ≈15°, corresponding to the direction of Drevja, for a couple of minutes around 15h05.